Alkaline electrolysis for green hydrogen production

A novel, simple model for thermo-electrochemical coupled system analysis

Jin, Lingkang; Nakashima, Rafael Nogueira; Comodi, Gabriele; Frandsen, Henrik Lund

Published in:
Applied Thermal Engineering

Link to article, DOI:
10.1016/j.applthermaleng.2024.125154

Publication date:
2025

Document Version
Publisher's PDF, also known as Version of record

Applied Thermal Engineering 262 (2025) 125154

Contents lists available at ScienceDirect

Applied Thermal Engineering

journal homepage: www.elsevier.com/locate/ate

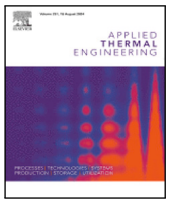

Alkaline electrolysis for green hydrogen production: A novel, simple model for thermo-electrochemical coupled system analysis

Lingkang Jin [a,*], Rafael Nogueira Nakashima [b], Gabriele Comodi [c], Henrik Lund Frandsen [b]

[a] Eindhoven University of Technology, Department of Electrical Engineering, Electrical Energy Systems, Eindhoven, 5600 MB, The Netherlands
[b] Department of Energy Conversion and Storage, Technical University of Denmark (DTU), Building 310, Fysikvej, DK-2800 Lyngby, Denmark
[c] Marche Polytechnic University, Department of Industrial Engineering and Mathematical Sciences, Ancona, Italy

ARTICLE INFO

Keywords:
Power-to-hydrogen
Alkaline electrolysis
Temperature control
Levelized cost of hydrogen
Hydrogen production

ABSTRACT

Alkaline water electrolysis (AWE) is the most mature electrochemical technology for hydrogen production from renewable electricity. Thus, its mathematical modeling is an important tool to provide new perspectives for the design and optimization of energy storage and decarbonization systems. However, current models rely on numerous empirical parameters and neglect variations of temperature and concentration alongside the electrolysis cell, which can impact the application and reliability of the simulation results. Thus, this study proposes a simple four-parameter semi-empirical model for AWE system analysis, which relies on minimal fitting data, while providing reliable extrapolation results. In addition, the effect of model dimensionality (i.e., 0D, 1/2D and 1D) are carefully assessed in the optimization of an AWE system. The results indicate that the proposed model can accurately reproduce literature data from four previous works ($R^2 \geq 0.98$), as well as new experimental data. In the system optimization, the trade-offs existing in the lye cooling sizing highlight that maintaining a low temperature difference in AWE stacks (76–80 °C) leads to higher efficiencies and lower hydrogen costs.

1. Introduction

The mass adoption of renewable energy sources, such as wind and solar, is the main pathway to mitigate the effects of climate change. However, the intermittent nature of these power sources creates an increasing demand for storage and management mechanisms. To address this challenge, the integration of green hydrogen production into the energy system emerges as a promising solution. Hydrogen offers advantages across various sectors, such as transportation, chemical and steel industries, as well as power systems [1]. Therefore, the European Union has established a framework to boost the adoption of renewable and low-carbon hydrogen, aiming to produce 10 million tonnes and import 10 million tonnes of renewable hydrogen by 2030 [2].

Green hydrogen can be produced by water electrolysis, a process that splits water into hydrogen and oxygen using electricity. Among the available technologies, alkaline water electrolysis stands out by its readiness and scalability for large-scale production, with an extended lifetime. However, alkaline water electrolysis exhibits lower efficiency, lower operating current densities, along with a constrained dynamic operating range compared with other technologies [3]. Thus, optimizing the technology design and operating conditions is essential to address the existing bottlenecks of alkaline electrolysis.

Both experimental and modeling investigations serve as essential tools in this regard. For instance, numerical models contribute to enhancing our understanding of various aspects of hydrogen production, including energy conversion efficiency, system sizing, thermal energy management, and optimization. In this context, alkaline electrolysis models can facilitate decision-making at the system level, such as energy systems investments and techno-economic evaluations. Thus, several past studies have proposed models for alkaline electrolysis, and Table 1 summarizes the most noticeable examples in the literature.

Among the works presented in Table 1, Ulleberg [5] stands out as an influential work on other models, such as Milewsk et al. [8] and Sanchez et al. [10].

In this model, the variation of cell voltage due to the current density and temperature is modeled by fitting six parameters. Similarly, subsequent works have proposed the use of more parameters (i.e., from 8 to 16) to include the effect of pressure on the cell voltage [10], capacitance of the double-layer effect [7] or to detail the overpotential contributions sources [11].

* Corresponding author.
E-mail address: l.jin@tue.nl (L. Jin).

https://doi.org/10.1016/j.applthermaleng.2024.125154
Received 15 April 2024; Received in revised form 25 September 2024; Accepted 3 December 2024
Available online 10 December 2024

Table 1
Review on alkaline electrolysis models for system analysis.

Reference	Fitting parameters	Temperature	Pressure	Concentration	Current density
Hug, et al. (1993) [4]	–	30-100 °C	1.01 bar	–	< 0.6 A/cm^2
Ulleberg (2003) [5]	6	30-80 °C	7 bar	30 wt% KOH	< 0.3 A/cm^2
Hammoudi, et al. (2012) [6]	–	23-80 °C	1.01-7 bar	30 wt% KOH	< 0.3 A/cm^2
Ursua et al. (2012) [7]	16	15-65 °C	25 bar	30 wt% KOH	< 0.4 A/cm^2
Milewsk, et al. (2014) [8]	5	70 °C	30 bar	8 M KOH	< 0.4 A/cm^2
Sandeep, et al. (2017) [9]	3	30-50 °C	–	30 wt% KOH	< 0.5 A/cm^2
Sanchez, et al. (2018) [10]	8	55-75 °C	5-7 bar	35 wt% KOH	< 0.5 A/cm^2
Haverkort and Rajaei (2021) [11]	14	27 °C	–	0.08-6 M KOH	< 1 A/cm^2
Jang, et al. (2021) [12]	–	80 °C	1.01 bar	30 wt% KOH	< 2 A/cm^2
De Groot et al. (2022) [13]	4	50-70 °C	10-55 bar	30 wt% KOH	< 0.7 A/cm^2

The large number of parameters may impose some challenges during the fitting procedure, such as difficult solution convergence or requiring more data for fitting. On the other hand, some authors have aimed to minimize the number of calibrated parameters by restricting the validation range (i.e., temperature, pressure, and concentration) [9], the geometrical characteristics of the electrolyzer [6], or the diaphragm material [13]. Although this modeling approach can simplify equations, the application range of the models can be limited by the fixed conditions imposed.

Additionally, alkaline electrolysis models often neglect the spatial variations of operating conditions and their impact on thermo-physical properties, such as density and specific heat. For instance, temperature fluctuations can affect voltage and current in cells, potentially leading to undesirable drops in performance. To ensure optimal performance, the flow rate of the liquid electrolyte can be adjusted to maintain the desired temperature, thereby efficiently dissipating the energy from water electrolysis. However, previous studies such as Jang et al. [12], have only analyzed the effects of temperature variation on the performance of the balance of plant due to the limited dimensionality of their electrolysis model (i.e., 0D). Careful consideration of temperature impact on overall efficiency and cost , including effects on electrochemical reactions, may be essential for the techno-economic optimization of alkaline electrolysis systems. On the other hand, integrating detailed multiphysics models of alkaline electrolysis with system-level simulations and optimizations may be unpractical, because they will require long computational times to be solved.

Thus, this study aims to address this research gap by proposing a novel, simplified, semi-empirical alkaline water electrolysis cell model, designed to be easily extendable to assess thermo-electrochemical coupling effects. The proposed model aims to make it easier to evaluate temperature dependencies within the alkaline electrolyzer system. To achieve this goal, a validated zero-dimensional/lumped model has been extended to a one-dimensional model that solves mass and energy conservation. This modeling approach is employed to evaluate and optimize system performance and cost under various inlet-outlet temperature differences.

The main contributions of this work are summarized below:

1. Propose and validate, with both previous literature and newly acquired experimental data, a semi-empirical alkaline water electrolysis model with four parameters, which can be applied to different types of alkaline electrolyzers.
2. Formulate a one-dimensional water electrolysis model, based on the physical process, by using ordinary differential equations. The model can assess the distribution of operational parameters, such as temperature and pressure, which are compared with models with reduced dimensions (i.e., 0D, 1/2D).
3. Techno-economic assessment and optimization of the temperature control, by varying the electrolyte flow rate, at a continuous range of inlet-outlet gap temperatures.

The paper is structured as follows: Section 2 describes the methodology adopted in this work, highlighting the proposed semi-empirical model and calibration methods. Section 3 reports the experimental data acquisition, followed by Section 4 and 5, describing the results obtained and conclusions, respectively.

2. Methods

In this section, a novel semi-empirical model for alkaline electrolysis, adopting four parameters is proposed, followed by a detailed description of the calibration process. Moreover, the extension into the one-dimensional model, assessing the coupling phenomena of electrochemical and thermal behavior, solving ordinary differential equations of mass, and energy balancing, is illustrated using a reference cell [5]. Finally, the techno-economic indicators adopted in this work, for the assessment of the effects of the temperature control, are explained and discussed.

2.1. Alkaline electrolysis and electrochemical modeling

Alkaline electrolyzers consist of one or multiple stacks, each equipped with electrochemical cells that can be electrically connected in series or parallel. Such cells' electrodes are partially submerged in liquid electrolyte that can either be Potassium Hydroxide (KOH) or Sodium Hydroxide (NaOH) based. For the electrolysis to take place, water and electricity are supplied to the cell, to initiate the electrolytic reaction, that splits the water molecules and as the products the hydrogen and oxygen gasses. The two electrodes' reactions are described in Eqs. (1a) (cathode reaction) and (1b) (anode reaction).

$$2H_2O + 2e^- \longrightarrow 2OH^- + H_2 \tag{1a}$$

$$2OH^- \longrightarrow \frac{1}{2}O_2 + H_2O + 2e^- \tag{1b}$$

The performance evaluation of the electrolysis process requires the perfect knowledge of the hydrogen produced and the electrical power consumed. While the first can be assessed through Faraday's law, which relates the hydrogen gas produced ($\dot{n}_{H_2}$) with the electrochemical cell's current (I_{cell}), as described in Eq. (2), the second is assessed indirectly through the polarization/I-V curve of the cell.

$$\dot{n}_{H_2} = \frac{I_{cell}}{2F} \tag{2}$$

Indeed, the polarization curve describes the relationship between cell current (I_{cell}) and voltage (V_{cell}). The cell voltage (V_{cell}) can be model as the sum of the reversible reaction voltage (V_{rev}) plus the overpotentials losses (η), as described in Eq. (3).

$$V_{cell} = V_{rev} + \eta_{act} + \eta_{ohm} + \eta_{bubble} \tag{3}$$

Nomenclature

Constants

F	Faraday constant, 96485 [C/mol]
LHV_{H_2}	H_2 Low Heating Value, 242 [kJ/mol]
R	Universal gas contant, 8.314 [J/mol K]

Subscripts

act	Activation
an	Anodic
$bubble$	Bubble formation
ca	Cathodic
$cell$	Cell level
d	Diaphram (electrolysis)
el	Electrolyte
H_2	Hydrogen
H_2O	Water
HEX	Heat exchanger
in	Inlet
O_2	Oxygen
OH	Hydroxide ions
ohm	Ohmic
out	Outlet
$pump$	Water pump
ref	Reference
rev	Reseversible
$stack$	Stack level
th	Thermo-neutral

Variables

α	Charge transfer coefficient, [-]
δ	Reaction distance, [cm]
$\dot{n}$	Molar flow rate, [mol/s]
$\dot{Q}$	Thermal power, [W]
ρ	Density, [kg/m^3]
σ	Ionic conductivity, [S/cm]
A	Area, [cm^2]
$CAPEX$	Capital Expenditure, [€]
CGR	Investment costs, [€]
Cp	Specific heat, [J/kg K] or [J/mol K]
CRF	Capital Recovering Factor, [-]
E	Energy, [kWh] or [Wh]
E_a	Activation energy, [J/mol]
H	Enthalpy, [J/mol]
I	Current, [A]
j	Current density, [A/cm^2]
k	Arrhenius scale factor, [A/cm^2]
$LCOE$	Levelised Cost of Energy, [€/kWh]
$LCOH$	Levelised Cost of Hydrogen, [€/kg$_{H_2}$]
M	Molarity, [mol/l]
m	Molality, [mol/kg]
MW	Molecular Weight, [g/mol]
P	Pressure, [bar] or [Pa]
p	Power, [W]
T	Temperature, [K] or [° C]
V	Voltage, [V]
w	Electrolysis cell width, [cm]
wt	Weight concentration, [0-1]

The reversible voltage (V_{rev}) represents the minimum electrical potential required for the reaction, while the overpotentials are irreversibilities that can be categorized into three main types: activation (η_{act}), ohmic (η_{ohm}) and concentration (η_{bubble}), in this case caused by the formation of gas bubbles.

2.1.1. Reversible voltage

For KOH-based electrolytes, the reversible voltage can be determined using equations (Eq. (4a)–(4h)), based on the work conducted by LeRoy et al. [14], Balej [15] and Ursua & Sanchis [7]:

$$V_{rev} = V_{rev,T} + \frac{RT}{2F}\ln\left(\frac{P - P_{v,\mathrm{KOH}}^{3/2}}{\alpha_{H_2O}}\right) \tag{4a}$$

$$V_{rev,T} = 1.5174 - 1.5421\cdot 10^{-3}T + 9.523\cdot 10^{-5}T ln(T) + 9.84\cdot 10^{-8}T^2 \tag{4b}$$

$$P_{v,\mathrm{KOH}} = \exp\left(2.302a + b\ln(P_{v,H_2O})\right) \tag{4c}$$

$$P_{v,H_2O} = \exp\left(81.6179 - \frac{7699.68}{T} - 10.9\ln(T) + 9.589110^{-3}T\right) \tag{4d}$$

$$\alpha_{H_2O} = \exp\left(-0.05192m + 0.003302m^2 + \frac{3.177\ m - 2.131m^2}{T}\right) \tag{4e}$$

$$m = \frac{wt_{\mathrm{KOH}}}{0.0561} \tag{4f}$$

$$a = -0.0151m - 1.678810^{-3}m^2 + 2.258810^{-5}m^3 \tag{4g}$$

$$b = 1 - 1.206210^{-3}m + 5.602410^{-4}m^2 - 7.822810^{-6}m^3 \tag{4h}$$

Where V_{rev} is calculated based on the Nernst equation, which is divided into two parts: the reversible potential ($V_{rev,T}$) at standard pressure (1 bar), and the effect of pressure under in non-ideal conditions [15]. The remaining equations involve empirical terms (a and b) and molality (m, in mol/kg) to determine the thermo-chemical properties: (i) equilibrium vapor pressure of $KOH_{(aq)}$ ($P_{v,\mathrm{KOH}}$, in bar), (ii) equilibrium vapor pressure of steam (P_{v,H_2O}, in bar) and (iii) chemical activity of water in $KOH_{(aq)}$ (α_{H_2O}). It is notable that these correlations are dependent on temperature (T, in K) and the concentration of KOH (wt, weight fraction). In addition, R and F represent the universal gas constant (in J/(mol.K)) and Faraday constant (in C/mol), respectively.

For NaOH-based electrolyte, the reversible voltage can be calculated by Eq. (5), assuming that the gases are wet and both electrodes share the same pressure [16].

$$V_{rev} = V_{rev,T} + \frac{RT}{2F}\ln\left(\frac{1.5\left(P - P_{v,H_2O}\right)}{P_{v,H_2O}}\right) \tag{5}$$

2.1.2. Activation overpotential

Activation overpotential is related to the kinetics of water electrolysis reaction in both electrodes. It has been observed that, under relatively high current densities (j, in A/cm^2) the activation overpotential of each electrode can be modeled by the Tafel equation, as stated in Eq. (6). Since separate electrode information is seldom available, an overall activation overpotential representing both electrodes is commonly used.

$$\eta_{act} = \left(\frac{1}{\alpha}\right)\frac{RT}{2F}\ln\left(\frac{j}{j_0}\right) \tag{6}$$

In Eq. (6), the charge transfer coefficient (α) is a fitted dimensionless parameter in the model. On the other hand, the exchange current density (j_0, in A/cm^2) is calculated by using the Arrhenius equation, as described in Eq. (7). This equation aims to model the influence of temperature in the kinetics of water electrolysis by introducing

two fitting parameters: a reference exchange current density ($j_{0,ref}$, in A/cm^2) and the activation energy (E_a, in J/mol).

$$j_0 = j_{0,ref} \exp\left(-\frac{E_a}{RT}\right) \rightarrow ln(j_0) = ln(j_0, ref) + \left(-\frac{E_a}{RT}\right) \quad (7)$$

2.1.3. Ohmic overpotential

The ohmic overpotential regards all voltages of the electrolyzer cell related to the electronic and ionic charge transport. The largest contributions for this loss are those related to the ionic charge transport across the liquid electrolyte and the electrolyzer diaphragm/separator. Thus, the ohmic overpotential can be estimated from the Ohm's law as described in Eq. (8), based on the conductivity of the liquid electrolyte (σ_{el}, in S/cm) and diaphragm (σ_d, in S/cm). In addition, since the electrolyte heavily influences ohmic losses and the diagram thickness (δ_d, in cm) may be unreported, Eq. (8) can also be simplified to use solely the electrolyte contribution calibrated by using an equivalent electrolyte length (δ_{el}, in cm).

$$\eta_{ohm} = j\left(\frac{\delta_{el}}{\sigma_{el}} + \frac{\delta_d}{\sigma_d}\right) \approx j\left(\frac{\delta_{el}}{\sigma_{el}}\right) \quad (8)$$

As regards the electrolyte ionic conductivity, Gilliam et al. [17] have proposed an empirical equation with the molarity (M, in mol/l) of KOH based solution and temperature, as reported in Eq. (9a). The liquid electrolyte density based on data reported by Ref. [17], as described in Eq. (9b), is used to estimate the molarity in Eq. (9c).

$$\sigma_{el} = -2.041M - 0.0028M^2 + 0.005332MT^2 + 207.2\frac{M}{T} + 0.001043M^3 - 3\cdot 10^{-7}M^2T^2 \quad (9a)$$

$$\rho = (5.1998\cdot 10^{-6}T^3 - 8.2381\cdot 10^{-3}T^2 + 3.2518T + 622)\exp(0.86wt_{\mathrm{KOH}}) \quad (9b)$$

$$M = \frac{C_{\mathrm{KOH}}}{56.1}\rho \quad (9c)$$

In the case of NaOH-based electrolyte, Le Bideau et al. [18] have proposed another empirical correlation, Eq. (10), based on the weight fraction of NaOH.

$$\sigma_{\mathrm{NaOH}(aq)} = 3.899\cdot 10^{-1} + 0.1914\cdot 10^{-2}(T + 273.15) + 9.993\cdot 10^{-5}wt_{\mathrm{NaOH}}^3 + 2.208\cdot 10^{-3}wt_{\mathrm{NaOH}}^2 + 3.564\cdot 10^{-2}wt_{\mathrm{NaOH}} \quad (10)$$

Regarding the diaphragm ionic conductivity, Vermeiren et al. [19] have performed tests on a 0.5 mm thick Zirfon-based diaphragm with KOH based solution at 30% weight concentration. From their results, is possible to have an empirical correlation for the σ_d at the temperature range of 20-80 °C. However, the diaphragm material can vary, therefore the empirical equation developed by Vermeiren is not suitable for all alkaline electrolyzers. Hence, in the proposed model, for the sake of the simplicity and generalization, the term δ_{el}, considered as an empirical parameter, includes both electrolyte and diaphragm ohmic contribution.

2.1.4. Four-parameters semi-empirical model

To summarize the previous sections details, highlighting the four distinct parameters, that need to be calibrated with the support of the experimental data, the polarization curve is described through Eq. (11).

$$V_{cell} = V_{rev} + \frac{1}{\boldsymbol{\alpha}}\cdot\frac{RT}{2F}\cdot\left(ln(j) - \left(\boldsymbol{ln(j_{0,ref})} + \left(-\frac{\boldsymbol{E_a}}{\boldsymbol{R}}\right)\cdot\frac{1}{T}\right)\right) + j\cdot\left(\frac{\boldsymbol{\delta_{el}}}{\sigma_{el}}\right) \quad (11)$$

Where the parameters are α (unitless), $ln(j_{0,ref})$ expressed in ln(A/cm^2), $-E_a/R$ with temperature unit (K) and δ_{el}, the reaction distance expressed in cm.

2.1.5. Bubble overpotential

The bubble overpotential is caused by the formation of bubbles in the liquid electrolyte at the reactive sites. Such bubbles could cause two effects. (i) Modification of the activation area of the cell, as the bubbles would cover a portion of it, and (ii) change of the electrolyte ionic conductivity. While the first effect would cause an increase of the overvoltage due to the activation, the last effect would cause an additional overvoltage for the ohmic part, since the parameters to be tuned are present in both effects (second and third term of Eq. (11)), the bubble effects are implicitly included during the calibration phase, with a variation of the parameters.

Since that from the modeling perspective, it is still a challenging task to capture its phenomena properly as it considers two different phases of the electrolyte (liquid+gas), despite many researchers' ongoing work [6,20,21]. Therefore, to directly capture the bubble formation physical complexity is far from being easy, and since it can be implicitly considered during the parameters tuning, thus, with the focus of this study to have a simple model for system analysis, as a compromise of the computational effort and physical details, the direct explanation of the formation of the bubble into the model is neglected.

2.2. Electrochemical model calibration and assessment

The model calibration, i.e. parameters tuning based on the experimental data, and the calibrated model performance assessment are disclosed in this section. Where during the first step, only a portion of the available data is used.

2.2.1. Calibration process

The ability of the proposed model to represent different measurements is further tested and calibrated in this work. This is done by using the experiments presented in the literature by different researchers from different types of alkaline electrolyzers with different set-ups of operating conditions. Such operating conditions are namely (i) temperature, (ii) electrolyte weight concentration, and (iii) pressure. Additionally, the model's robustness, i.e. its ability to have reasonable accuracy, using the minimum amount of the data available, has been also tested.

The calibration procedure of the model is illustrated in Fig. 1. It can be divided into 3 steps:

1. Process the data acquired, ensuring at least six data points, spanning two different temperatures, to ensure accurate modeling. Additional data points may also be included.
2. Calibrate the model to the data, using a curve-fitting framework, commonly used ones are Matlab and Python, adopting the proposed model, assessing the four open parameters (δ_{el}, α, $-E_a/R$, $ln(j_{0,ref})$).
3. Reproduce the polarization curves at different temperatures.

During the parameter estimation process, the dataset is split into two separate datasets. To prove the model's robustness and avoid the over-fitting behavior. Indeed, the training dataset, i.e. the data used to find parameters, is randomly selected. A constraint for the use of a data set is that at least six data points are present, from at least two different operating temperatures.

2.2.2. Model performance indicators

To compare the effectiveness and the robustness of the calibrated model, several data-science prediction performance indicators are adopted, such as Mean Average Error (MAE), Mean Average Percentage Error (MAPE), Root Mean Squared Error (RMSE) and Coefficient of determination/R^2.

Where for each dataset, at a given temperature, the cell voltage vector, that has n values $[V_{cell,1}, \ldots, V_{cell,n}]$, each associated with a predicted value using the calibrated model, $[\hat{V}_{cell,1}, \ldots, \hat{V}_{cell,n}]$, the performance indicators are defined in Eqs. (12a)–(12e).

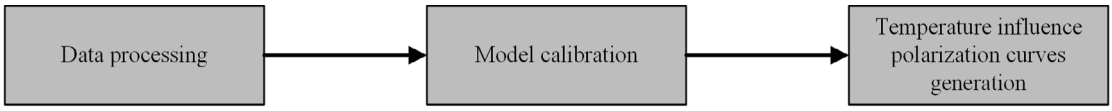

Fig. 1. Parameters estimation procedure. Divided into three steps: (1) collection of experimental data at different temperatures, (2) parameter estimation, and (3) generation of polarization curves at different temperatures.

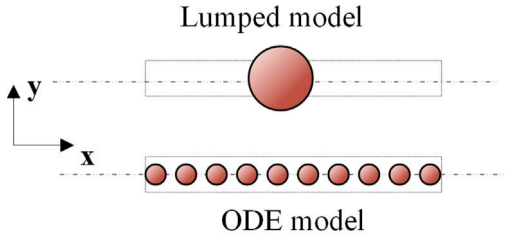

Fig. 2. Thermal model differences: Lumped model vs discretized ODE.

$$\overline{V}_{cell} = \frac{1}{n}\sum_{i=1}^{n} V_{cell,i} \tag{12a}$$

$$MAE = \frac{1}{n}\sum_{i=1}^{n} |V_{cell,i} - \hat{V}_{cell,i}| \tag{12b}$$

$$MAPE = 100 \cdot \frac{i=1}{n}\left|\frac{V_{cell,i} - \hat{V}_{cell,i}}{V_{cell,i}}\right| \tag{12c}$$

$$RMSE = \sqrt{\frac{i=1}{n}\sum_{1}^{n}\left(V_{cell,i} - \hat{V}_{cell,i}\right)^2} \tag{12d}$$

$$R^2 = 1 - \frac{\sum_{i=1}^{n}\left(V_{cell,i} - \hat{V}_{cell,i}\right)^2}{\sum_{i=1}^{n}\left(V_{cell,i} - \overline{V}_{cell}\right)^2} \tag{12e}$$

2.3. Electrochemical and thermal coupling

The thermal behavior of electrolysis directly influences the efficiency of hydrogen production. Hence, an exhaustive mass and heat transfer model is essential to accurately capture the response of the electrolyzer.

Since lumped models treat the entire stack as a single point and cannot capture temperature distribution and evolution (Fig. 2), a more advanced approach is likely needed. In this study, the Partial Differential Equations (PDE) along the flow direction are solved using several simplifications and compared to the typically used lumped approach. The following simplifications are made:

- The engineering of the stack ensures that each of the cells experiences more or less the same flow, and the stack can thus be represented by the modeling of a single repeating unit;
- Uniform flow across each cell is also ensured, such that a single cell can be represented by considering only variations in the flow direction (a single flow channel);
- The variations within the flow channel are accounted for by the semi-empirical cell model, in particular reaction distance δ_{el};
- Finally only a steady state is considered.

With these assumptions and simplifications, the stack can be represented with a 1D model describing the variations of species, reaction rates, and temperature in the flow direction. Consequently, the mass and energy balance partial differential equations are simplified to a set of ordinary differential equations:

$$\frac{d\dot{n}_{H_2}}{dA} = \frac{j}{2F} \tag{13a}$$

$$\frac{dT}{dA} = \frac{(V_{cell} - V_{th})j}{\dot{n}_{el}cp_{el} + \dot{n}_{H_2}cp_{H_2} + \dot{n}_{O_2}cp_{O_2}} \tag{13b}$$

The 1D model is solved by use of the finite volume method, where mass and energy balances are ensured within each volume. This refined model enables the assessment of variations in temperature and electrolyte concentration along the flow direction (x axis). Furthermore, this model is expanded to the stack level, built upon the electrical arrangement of the cells, as depicted in Fig. 3.

For each volume all thermo-electrochemical properties are updated to describe the variation along the electrolyte flow direction (x axis). Consequently, the mass and energy balance differential equations are solved along the electrolyte flow axis, volume by volume:

$$\dot{n}_{H_2,i} = \dot{n}_{H_2,i-1} + \frac{j_i}{2F}\Delta A_i \tag{14a}$$

$$T_i = T_{i-1} + \frac{(V_{cell} - V_{th})j_i}{\dot{n}_{el}cp_{el} + \dot{n}_{H_2}cp_{H_2} + \dot{n}_{O_2}cp_{O_2}}\Delta A_i \tag{14b}$$

$$i = 1, 2, 3, \ldots, n_{elements} \tag{14c}$$

In each element (i), the molar flow rate and thermal balance are determined, considering a small finite cell area (ΔA_i). As depicted, both equations rely on inputs from the electrochemical calculations. Moreover, the temperature outcomes from these equations are subsequently used in the next element, as boundary conditions, for electrochemical assessments.

2.3.1. Mass conservation and weight concentration variation

The Eq. (14a) describes the molar mass variation due to the electrolysis process. And it can be extended further for the weight concentration variation assessment.

$$H_2O \leftrightarrow H_2 + \frac{1}{2}O_2 \longrightarrow \Delta\dot{n}_{H_2} = \Delta\dot{n}_{H_2O} = \frac{1}{2}\Delta\dot{n}_{O_2} \tag{15}$$

$$wt = \frac{\dot{m}_{KOH}}{\dot{m}_{KOH} + \dot{m}_{H_2O}}; (1 - wt) = \frac{\dot{m}_{H_2O}}{\dot{m}_{KOH} + \dot{m}H_2O} \rightarrow \frac{\dot{m}_{KOH}}{wt} = \frac{\dot{m}_{H_2O}}{1 - wt} \rightarrow \dot{m}_{KOH} = \dot{m}_{H_2O} \cdot \frac{wt}{1 - wt} \tag{16}$$

$$\dot{m}_{KOH} = \frac{wt}{1 - wt} \cdot \dot{m}_{H_2O,i=1} = \frac{wt}{1 - wt}\dot{n}_{H_2O,i=1} \cdot MW_{H_2O} \tag{17}$$

Specifically, given the chemical reaction of the electrolysis (Eq. (15)), the molar rate of the hydrogen produced is equal to the molar flow rate of the water consumed. Based on the weight concentration definition (Eq. (16)), the KOH mass flow, assumed to be constant over the stack, can be assessed given the inlet water flow rate ($\dot{m}_{H_2O}$), illustrated in Eq. (17). Therefore the weight concentration variation over the cell can be described through Eq. (18), with the water molar flow rate variation described in Eq. (19).

$$wt_i = \frac{\dot{m}_{KOH}}{\dot{m}_{KOH} + \dot{n}_{H_2O,i} \cdot MW_{H_2O}} \tag{18}$$

$$\dot{n}_{H_2O,i} = \dot{n}_{H_2O,i-1} - \Delta\dot{n}_{H_2O} = \dot{n}_{H_2O,i-1} - \Delta\dot{n}_{H_2} \tag{19}$$

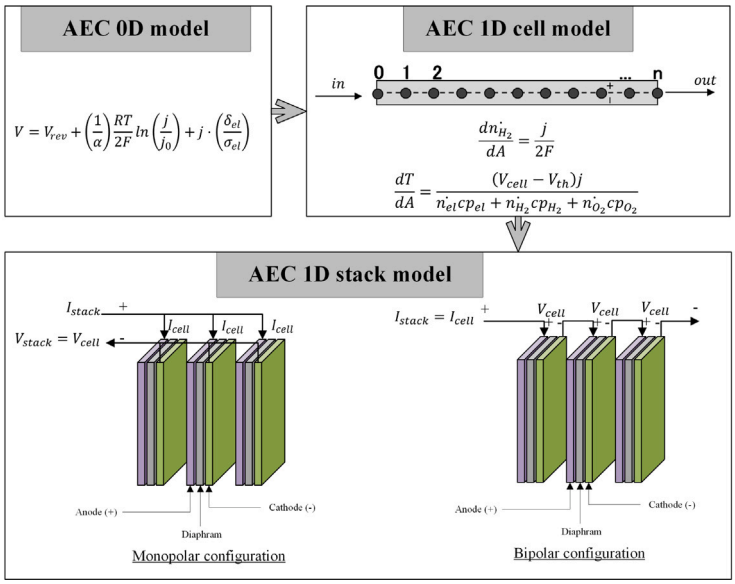

Fig. 3. Alkaline 1D stack model simulation flowchart. Starting with the single cell 0D model, extended to the 1D cell model, solving mass and thermal balance, and finally 1D stack model, based on the electrical configuration among cells.

2.3.2. Thermal energy balance

For the temperature variation assessment, when considering standard chemical species, their thermodynamic properties, including specific heat (c_p), can be derived using empirical correlations available in databases such as the one from NASA [22]. However, for the electrolyte, its properties vary considerably with weight fraction, as demonstrated in experiments reported by Le Bideau et al. [18]. For this study, the Zaytsev empirical relationship, that is valid for both KOH and NaOH-based electrolytes, has been employed to account for these variations [23].

$$cp_{el,mass} = 4.236 \cdot 10^3 + 1.075 ln\left(\frac{T-273}{100}\right) + \left(-4.831 \cdot 10^3 + 1.576 \cdot 10^3 wt + 8(T-273)\right) wt \quad (20)$$

The specific heat obtained is expressed in [J/kg K]. As all the balances are molar-based, it is necessary to convert this mass-based specific heat into a molar-based one [J/mol K]. This conversion can be achieved using the Eqs. (21a)–(21d), where k indicates the number of chemical species.

$$cp_{el} = cp_{el,mass}\frac{MW_{el}}{1000} \quad (21a)$$

$$wt_k = \frac{n_k MW_k}{m_{tot}}; m_{tot} = n_{tot} MW_{tot}; n_{tot} = \sum_k n_k \quad (21b)$$

$$\sum_k \frac{wt_k}{MW_k} = \frac{1}{MW_{tot} n_{tot}} \frac{n_k MW_k}{MW_k} \quad (21c)$$

$$MW_{tot} = \frac{1}{\sum_k \frac{wt_k}{MW_k}} \rightarrow MW_e = \frac{1}{\frac{wt}{MW_{KOH/NaOH}} + \frac{(1-wt)}{MW_{H_2O}}} \quad (21d)$$

The flowchart of the proposed 0D/lumped electrochemical model, along with its extension to the 1D cell model using the ODE approach for thermal behavior, and further into the 1D stack model, is illustrated in Fig. 3.

The comparison of thermo-electrochemical models at different scales has been conducted, encompassing three distinct domain-scale models. These models were developed utilizing the potentiostatic approach, which involves providing the cell's voltage as input data.

- 0D model, or lumped model, only a single point is considered for the whole cell, defined as follows:

$$0D: T_{in}; j = j_{in} = f(T_{in}, V, wt, P) \quad (22)$$

- 1/2 D model assumes that the distribution of current density alongside the cell area is linear and, therefore, the average current density can be determined as the mean value between inlet and outlet states, as stated in Eq. (23). Since the outlet state is unknown, an iterative process using a root-finding algorithm (e.g. Newton or secant method) is employed to determine the outlet state (i.e., j, T, n_i, etc.) that converges to the fixed value of j_{avg}.

$$1/2D: T_{in}, T_{out}: j = j_{avg} = \frac{j_{in} + j_{out}}{2} \quad (23)$$

- 1D model is the model using ODE previously mentioned. It allows having information for discrete volumes through the stack, as reported in the following equations :

$$1D: T_i; i = 1, \ldots, n_{elements}; j = j_{avg} = \frac{\sum_{i=1}^{n_{elements}} j_i}{n_{elements}} \quad (24a)$$

$$\Delta A = \frac{A_{cell}}{n_{elements}} \quad (24b)$$

2.3.3. Numerical code implementation

The whole model was implemented in *Python* environment [24], where several dedicated open-source libraries are adopted. Specifically, *Pandas* [25] for the data management, *Scipy* [26] for the calibration of the model (i.e. find out the parameters), solving the inverse functions and solving the finite volume equations, while *Scikit-learn* [27] is used for the assessment of the performance indicators. Furthermore, the implementation of the 1D model can be find in the pseudo-code structure in Algorithm 1.

Since initial input regards the inlet temperature, rather than the outlet-inlet temperature difference. When the goal is to set the temperature difference, the initial water flow rate is computed by solving iteratively the algorithm, such as to get the desired gap temperature, through *Scipy* module *fsolve*, which allows finding the roots of nonlinear functions.

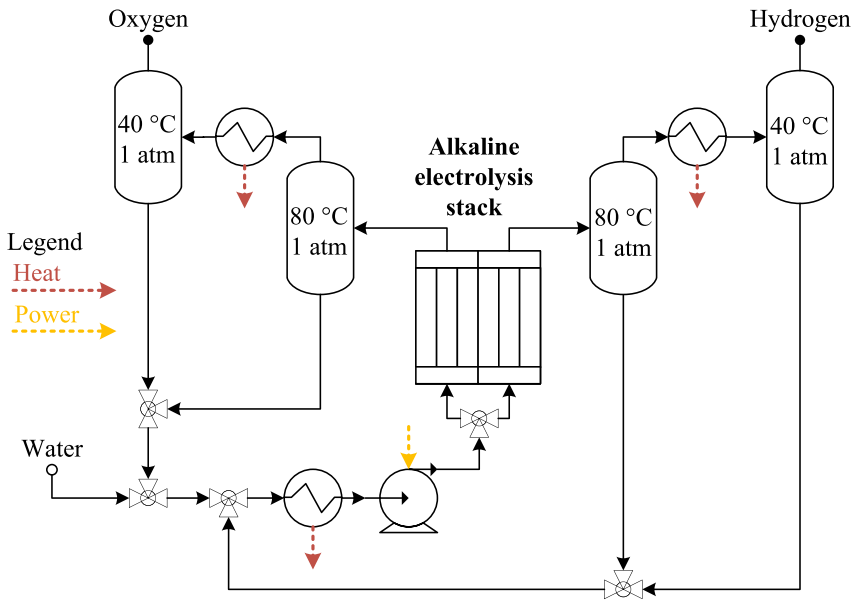

Fig. 4. Flow diagram of the alkaline electrolyzers systems, illustrating auxiliary components coupled with electrolyzer stack.

Algorithm 1 Algorithm of finite volume model ($\frac{d...}{dA}$)

1: **Input:** Calibrated cell model, inlet voltage, temperature, pressure, and weight concentration
2: **Output:** Temperature, hydrogen production, water consumption, and weight concentration variation
3: Initialize vectors for $T_{cell,i}$, $\dot{n}_{H_2,i}$, $\dot{n}_{H_2O,i}$, wt_i
4: **for** i in $n_{elements}$ **do**
5: Assess electrolyte properties (Cp_{el}, MW_{el}, $\dot{n}_{el}$)
6: Find the current density given the V_{cell},$T_{cell,i}$ p, wt_i , through solving the inverse calibrated polarization curve (j_i).
7: Assess the reaction rate for the element on Faraday law ($\Delta\dot{n}_{H_2,i}$,$\Delta\dot{n}_{H_2O,i}$)
8: Assess all species' thermal properties and evaluate the temperature increase (ΔT_i)
9: **end for**
10: **return** ΔT_i,$\Delta\dot{n}_{H_2,i}$,$\Delta\dot{n}_{H_2O,i}$, wt_i
11: Solve the loop over A using *Scipy* dedicated module for integrals.

2.4. System level approach: temperature control

Another key perspective of having such a model is the possibility of determining its integration with other plant components and gaining insights into an optimal operational strategy. For this study, temperature control and its effects on both technological and economical perspectives, have been assessed. The data regarding the components specifications can be found in Table 2. The whole alkaline electrolyzer stack can be connected with all necessary auxiliary components, as illustrated in Fig. 4.

To compare determine which electrolyte flow rate is optimal, the system efficiency and the levelized cost of hydrogen are determined and compared for different flow rates. As evaluation indicators, exploiting the temperature effects, system-level efficiency and the levelized cost of the produced hydrogen ($\dot{m}_{H_2}$) are adopted.

$$\eta_{tot} = \frac{N_{cells}\dot{n}_{H_2,cell}LHV_{H_2}}{p_{stack} + p_{pump}} \tag{25a}$$

$$LCOH = \frac{C_{GR}CRF + E_{el}LCOE + R + L + OPEX_o}{\dot{m}_{H_2}t_{year}} \tag{25b}$$

Where all investment costs (C_{GR}), that depend on the nominal size of each component, are discounted in annual costs by using a capital recovery factor (CRF) [34]. In addition, E_{el} is the electrical energy consumption and LCOE is the levelized cost of electricity. R and L account for the replacement cost of the electrolysis stacks and operating labor, respectively. $OPEX_o$ represents other operating costs, such as taxes, insurance and overhead. Finally, the full load operating hours (t_{year}) is assumed as 50% of total hours in a year [30].

3. NaOH-based electrolyzer experimental data

The experimental data, which regards a NaOH-based electrolyte alkaline electrolyzer, is collected from the hydrogen lab of Marche Polytechnic University (Fig. 5), is acquired for further calibration of the proposed semi-empirical model. Such lab configuration allows the assessment of the system-level analysis of the complete hydrogen value chain, incorporating the water demineralization, hydrogen production through the alkaline electrolyzer, hydrogen gas purification and dehumidification, compression and storage (in metal hydrides), and lastly the utilization of the hydrogen through a fuel cell. However, technology-level analysis of each system (for instance the stack level) is not possible as it would cause overrides and impact the whole lab's balance of the plant. Further details can be found in Fig. 6, where each key component of the lab and the energy flows are disclosed. The completeness of the hydrogen lab guarantees an overview of the different systems and their interconnection impacts. Yet, each system can be analyzed in detail separately, indeed the scope of the works is focused solely on the alkaline electrolyzer.

The data acquired regards the normal operation of the whole lab, at the ambient temperature (approximately 20 °C). which consists of hydrogen production, purification, compression, storage, and utilization at the same time, such setup is mainly for data acquisition and monitoring, with the aim to use the collected data for the calibration of the systems and models, and analyze the impacts of their interconnection. Given the focus of the work, only the data regarding the alkaline electrolyzer is disclosed. Specifically, the normal operation of means that the electrolyzer would ramp up to the nominal pressure, heat up the electrolyte finally reach the nominal production rate, and keep the nominal hydrogen production until the storage system is full, controlled by the pressure valve, and goes in a stand-by mode, and back to production when the storage pressure drops to a target lower threshold. The electrolyzer data is acquired through the

Table 2
Modeling parameters for alkaline water electrolysis temperature control.

Description	Value	Ref.
Electrolysis stack		
Cell area - A_{cell} [m^2]	2.5	[28]
Number of cells - N_{cell} [-]	8000	
Pressure [bar]	7	[5]
Max. Temperature [° C]	80	[5]
Specific bare module cost [€/m^2]	1575	[29]
Stack lifetime - n_{life} [y]	10	[30]
Present value replace cost - R [€]	$1575 \cdot A_{cell} N_{cell}/(1-i')^{n_{life}}$	[30]
Cost reference year	2023	[29]
Rectifier		
Efficiency (%)	95	[31]
Specific bare module cost [USD/kW]	130	[32]
Exchange rate - 2018 [€/USD]	1.18	[33]
Cost reference year	2018	[32]
Lye cooler		
Type/Material	Plate/Stainless steel	
Overall heat transfer coefficient [W/m^2.K]	850	[34]
Cooling water inlet/outlet temperature [° C]	27/45	[34]
Temperature correction factor	0.8	[34]
Heat exchange area - A_{hx}	$A_{hx} = Q/(U_{hx} T_{lm} F)$	[34]
Purchased cost - PEC [USD]	$10^{(4.666-0.156\log_{10}(A_{hx})+0.155(\log_{10}(A_{hx})^2)}$	[34]
Bare module cost - C_{BM} [USD]	$3.864 \cdot PEC$	[34]
Exchange rate - 2001 [€/USD]	1.1	[33]
Cost reference year	2001	[34]
Lye pump		
Type/Material	Centrifugal/Stainless steel	
Efficiency (%)	70	[34]
Pressure difference [bar]	0.3	[10]
Purchased cost - PEC [USD]	$10^{(3.389+0.054\log_{10}(P)+0.154(\log_{10}(P)^2)}$	[34]
Bare module cost - C_{BM} [USD]	$4.86 \cdot PEC$	[34]
Exchange rate - 2001 [€/USD]	1.1	[33]
Cost reference year	2001	[34]
Grassroot costs - C_{GR}	168% $\sum C_{BM,i}$	[34]
Manufacturing costs		
Number of hired operators - N_{op}	12	[34]
Operator salary - S_{op} [€/y]	64 400	[35]
Labor - L [€/y]	$N_{op} S_{op}$	[34]
Other operating expenses - $OPEX_o$ [€/y]	9% C_{GR} + 125% L	[36]
Others		
Interest rate - i	8%	
Inflation rate - f	2%	[37]
Effective interest rate - i'	$(i-f)/(i+f)$	[34]
Full load operating hours - t_{year}	4380	[30]
Levelized cost of electricity - LCOE [€/MWh]	30–60	

Fig. 5. Hydrogen lab at Universita' Politecnica delle Marche.

Table 3
ERREDUE G6 alkaline electrolyzer technical data.

System data	
Power [kW]	23
Current [A]	40
Pressure [bar]	4
Voltage [Vac]	3x 400 +Neutral
Production	
Hydrogen flow rate [Nm^3/h]	4
Hydrogen purity [%]	99.3–99.8
Oxygen flow rate [Nm^3/h]	2
Oxygen purity [%]	98.5–99.5
H_2O spec.	
Max. conductibility [$\mu S/cm$]	5
Max. consumption [lt/h]	3.4
Cell-to-Stack	
Electrical configuration	Bipolar
#n stacks	2
#n total cells	160
Cell area [cm^2]	450

Human–Machine Interface, tailored for the customized application of the system, which communicates, through Modbus protocol, directly with the PLC controller of the machine. Specifically, the controller of the machine is a PLC controller from ABB series AC500 [38], while the monitored and saved data are the following ones:

1. Pressures, from both hydrogen and oxygen gasses and also the system equilibrium pressure. Where slight deviation can be present among them.
2. Temperatures, of the stacks and the liquid electrolyte.
3. Gasses flow rate, from both hydrogen and oxygen.
4. System level current and voltage.

The electrolyzer is a G6 model from the manufacturer *ERREDUE* [39], using 18%wt NaOH (Sodium Hydroxide) based electrolyte, with a nominal production capacity of 4 Nm^3/h with a maximum operating pressure of 4 bar, and a nominal electrical power of 23 kW. Furthermore, it is composed of two stacks connected in series, achieving overall 160 cylindrical cells, each of them with 450 cm^2 of cell area. Further specification details are illustrated in Table 3.

Using NaOH, instead of KOH-based electrolyte, changes the electrolyte's thermophysical properties. Such as density, molecular weight (56.1 g/mol for KOH, 39.997 g/mol for NaOH), and specific heat coefficient, while the electrochemical equations remain mostly the same. Fortunately, such properties can be assessed through the empirical relationships, based on the temperature and electrolyte concentration, that are validated by other researchers, and reported in the review done by Le Bideau et al. [18].

4. Results and discussion

In this section, results regarding the calibration of the semi-empirical model, both from literature data (four different datasets) and acquired experiments are presented. Furthermore, a technological and economical analysis, from a system-level perspective, assessing the temperature influence, through the use of the 1D model, is also reported.

All results are performed with the hardware of 12th Gen Intel(R) Core(TM) i7-12700H CPU at 2.30 GHz with 16 GB RAM, which completes the whole finite volume analysis and dimensionality comparison in approximately 12 seconds, proving the efficient and simple nature of the model. However, this comes with a good estimation of the initial guesses of the inversed function (current density, and water flow rate), which can be only tuned based on the try and error method, as wrong/no initial guesses could cause no convergence of these functions.

4.1. Model calibration: Literature data

Four different datasets from the literature have been used, all of them adopting the KOH-based electrolyte, yet operating under different pressures, concentrations, and temperatures, not to mention their geometrical diversity. These datasets are extracted from the following references: Sakas [28], Ulleberg [5], Sanchez [10] and De Groot [13]'s work.

The results of the estimation, illustrating the model's wide applicability, are reported in Fig. 7. Whereas the temperature dependence is explicitly highlighted, in activation overpotential, other operating conditions influence, namely KOH weight concentration and pressure are implicitly considered, through the ohmic overpotential and reversible voltage, respectively.

As shown in Fig. 7, the proposed model four-parameter model adequately represents the data ($R^2 > 0.98$) of the variety of electrolyzers. Moreover, it is important to note that not all available experimental data were utilized for parameter determination, and the training dataset was randomly selected. and as an indication of the model's robustness, all performance indicators are reported in Table 5, with a maximum MAE of 0.0092 V, MAPE of 0.55% and a RMSE of 0.00013 V.

4.2. Model calibration: NaOH based electrolyte experimental data

A dedicated calibration of the Marche Polytechnic University electrolyzer data is reported, not only because of the difference of the type of the electrolyte, adding an additional level of the model's generalizability, compared with ones of literature, but also to highlight some insights during the acquisition of these data. However, to the best of the author's knowledge, no literature data regarding the NaOH-based electrolyzers were available, which was the difficulty raised in [40]. Thus, no range of parameters can be determined for such type of electrolyte-based electrolyzer, differently for the KOH-based ones.

For experimental setup, the electrolyzer is configured so that it can produce the maximum amount of hydrogen, and this can be done with the following sequential steps:

1. Pressurize the system, until it reaches the target pressure.
2. Heat up the electrolyte using the thermal energy generation from the electrolysis process. However, such temperature ramping is a slow process, that could take from 30 min to hours.
3. Reach the nominal hydrogen production rate at the nominal conditions when both temperature and pressure are at their target value.

The parameters are acquired dynamically during the lab test, meaning that the pressure and temperature are acquired as time series, as illustrated in Fig. 8. Indeed, both temperature and pressure vary rather than being constant.

4.2.1. Experimental data processing

For the experimental set-up considered in this study, since all operational parameters are acquired dynamically, during a normal operation of the electrolyzer, consequently, several pre-processing steps for the data acquired are required, which are:

- Temperature and pressure categorization: Given the continuous nature of the monitored time-series data, these parameters must be discretized into appropriate bin widths. For temperature, a bin width of 5 °C is used.
- Data cleaning and outlier removal: This step addresses anomalies caused by noise during data acquisition, such as removing data with non-physical values (e.g., temperatures below ambient levels or unusual voltage spikes).

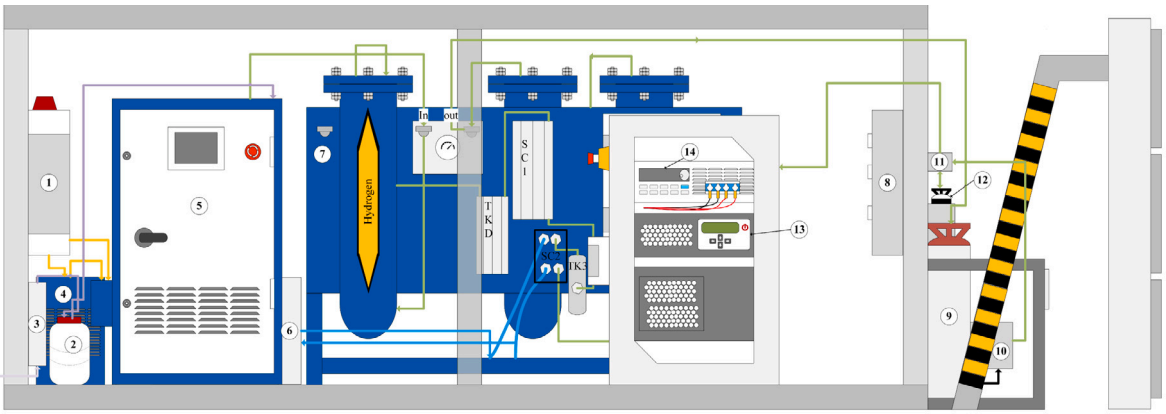

#n	Description	Comment
1	Electrical Cabinet	Main cabinet
2	Water tank	with water level sensor
3	Demi system	Water conducibility<5$\mu S/cm$
4	Electrolyzer rectifier	AC/DC converter
5	Alcaline electrolyzer	23 kW, 4 Nm3, NaOH based electrolyte
6	Chiller	Hydrogen cooling system
7	DPSH6/Hydrogen purification	Purification using condensation process: • 3 hydrogen tanks • 2 hydrogen cooling system (first air cooling then chiller cooled), both after first hydrogen tank

#n	Description	Comment
8	Electrical Cabinet	Controls hydrogen storage
9	Hydrogen buffer tank	10l volume, P~3-5 bar
10	Booster/Hydrogen compressor	Pneumatic driven, max H2 pressure 30 bar
11	Hydrogen line collector	Communal node to metal hydrides and fuel cell
12	Hydrogen storage	2X metal hdyrides tank with water conditioning
13	PEM FC	1 kW PEM fuel cell
14	Controllable electronic load	Analogic control, 1 kW, Controlled in Current, while voltage~55-56 V

Type	Carrier	Comment
	Compressed air	6-8 bar, using an air compressor
	Electricity	Grid connection
	Demi Water	Conducibility< 5$\mu S/cm$
	Chiller refrigerant	Cooling vector in SC2
	Network water	Not demineralized
	Hydrogen	Different pressure over the line: • 4-5 bar at electrolyzer outlet • 4-5 bar at DPSH6 outlet • Max 30 bar from booster outlet • 5 bar at first reduction valve • 0.55-0.7 bar at PEMFC inlet

Fig. 6. Hydrogen lab layout and systems description.

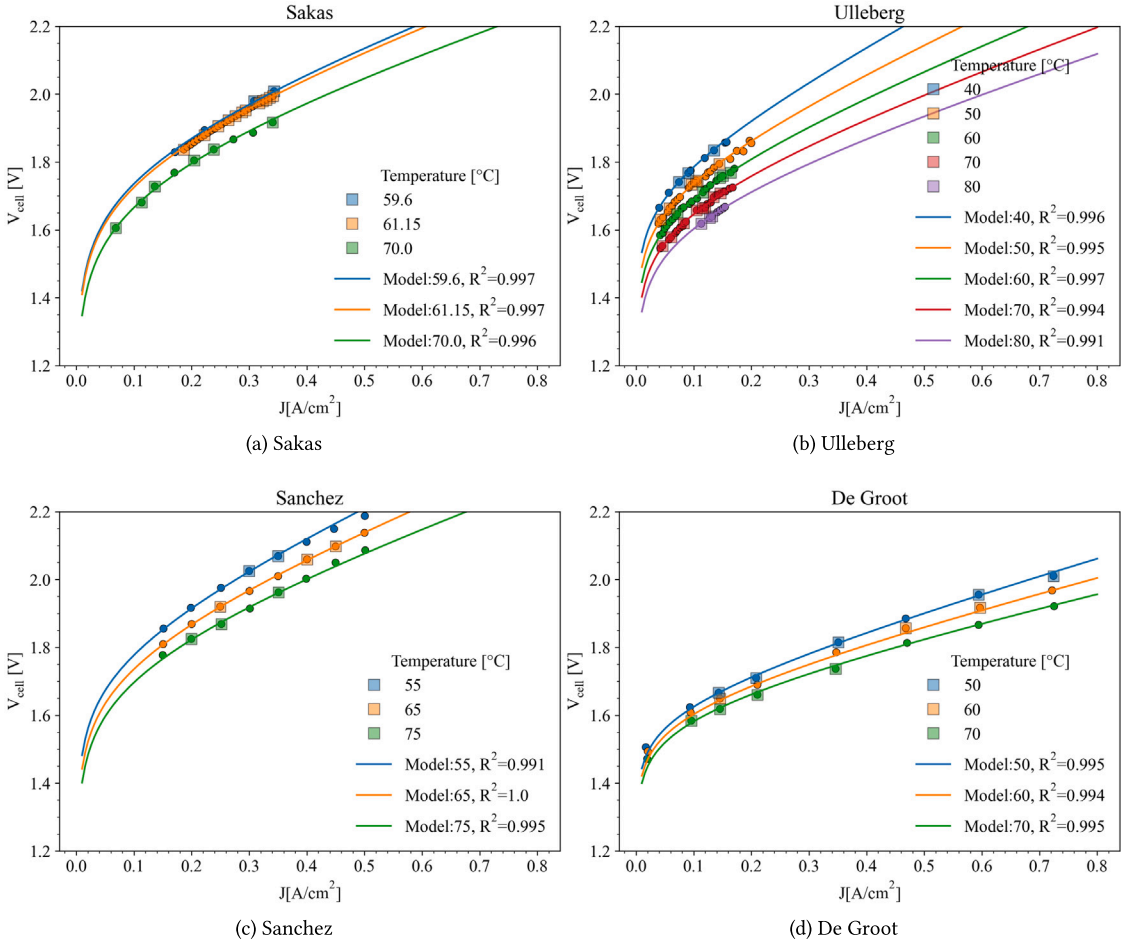

(a) Sakas (b) Ulleberg

(c) Sanchez (d) De Groot

Fig. 7. Parameters estimation and validation with temperature variation. Where squared-dotted data are from the training dataset, while the others are from the test dataset.

- Convert system-level data to cell-level data to better discern voltage differences across temperatures and ensure consistency with the semi-empirical model calibration. This is done by using the cell area and the number of cells connected in series to form the electrolyzer. For the electrolyzer examined, the cell area was 450 cm^2 with 160 cells. (see Fig. 9).

Table 4
Semi-empirical model validation: Despite different operational conditions, parameters' ranges are similar.

Electrolyte	Experimental conditions			Calibrated parameters			
KOH	p [bar]	T [° C]	wt [-]	δ_{el} [cm]	α [-]	$\frac{-E_a}{R}$ [K]	$ln(j_{0,ref})$ [ln($\frac{A}{cm^2}$)]
Sakas	16	59.6-61.15–70	0.25	0.54	0.12	−6441	13.46
Ulleberg	7	40-50-60-70-80	0.30	0.52	0.15	−5290	9.34
Sanchez	7	55-65-75	0.35	0.67	0.14	−4128	4.77
De Groot	30	50-60-70	0.28	0.41	0.25	−3395	3.23
Parameters range				[0,1]	[0,0.4]	[−8000,-3000]	[0,15]

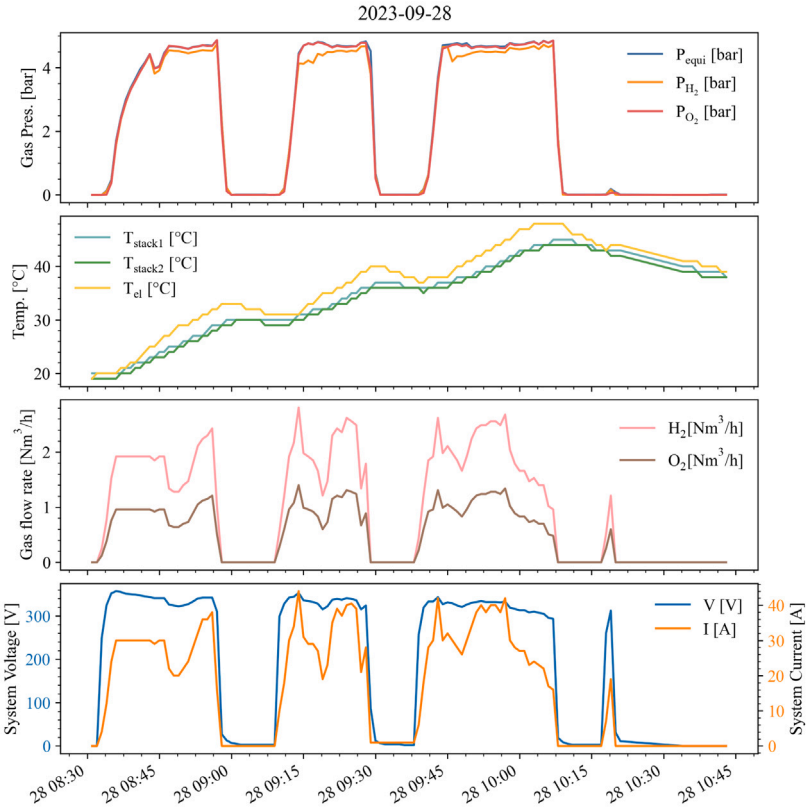

Fig. 8. *ERREDUE* G6 23 kW electrolyzer acquired data of (i) pressures of gasses, (ii) temperatures, (iii) produced gasses flow rate, and (iV) voltage and current of the system.

4.2.2. Experimental data calibration

After the data processing stage, the experimental data can be calibrated with the same procedure as the literature data (see Table 6.). Where comparing with them , despite having different electrolytes, which results in a poorer performance, comparing polarization curves, the *ERREDUE* electrolyzer is qualitatively comparable with KOH-based ones.

Where Fig. 10 illustrates the validation of the model with the acquired time series data. Due to noise presence in the data, the R^2 is lower, compared with literature-based datasets. The model does however still qualitatively reasonably represent the recorded data, with a maximum MAE of 0.016 V, MAPE of 0.78%, RMSE of 0.0003 with $R^2 \geq 0.81$, as reported in Table 7.

4.3. Model dimensionality comparison

Given the 1-D model has the potential to assess multiple parameters along the flow direction inside the alkaline stacks, thus, it serves as the reference due to its higher accuracy for the comparison. Fig. 11 illustrates the difference between models with varying dimensionality. Where current density is taken as a comparison indicator, at a fixed potential of 1.8 V. This comparison is conducted under various electrolyte flow rates through the stack for cooling, leading to different temperature increases across the stack.

The results of the comparison indicate that the 0D model, the most adopted one, showcases a substantial deviation from the 1-D model's current density and, consequently, the hydrogen production rate. However, the 1/2D model shares almost the same results as the 1D model, and it starts to deviate from it at higher temperature gaps.

4.4. System level temperature control and effects

The reference cell model was consequently assumed to be able to represent a full stack, which was embedded in the alkaline electrolysis system shown in Fig. 4. This system was then operated to control the temperatures across the stack, by adjusting the electrolyte flow rate by pumping. The purpose is to investigate if increased pumping and consequent temperature leveling inside the stack will increase or decrease the overall system efficiency.

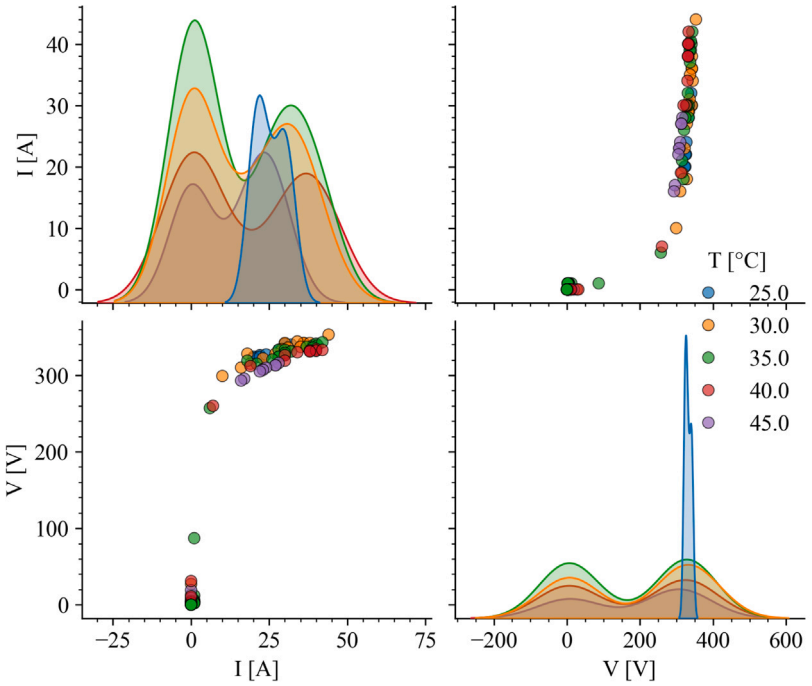

Fig. 9. Scatter-plots and Kernel Density Estimation of the current and voltage of the electrolyzer, categorized based on the temperatures, as can be seen, it is not easy to see the voltage difference over different temperatures.

Table 5
Calibrated model performance at different temperatures, for each dataset.

	MAE [V]	MAPE [%]	RMSE [V]	R_2 [–]
Sakas		$p = 16$ bar		
59.6 °C	0.0026	0.14	1.32e−05	0.997
61.15 °C	0.0017	0.09	5.77e−06	0.997
70 °C	0.0052	0.29	4.08e−05	0.996
Ullerberg		$p = 7$ bar		
40 °C	0.0016	0.09	5.27e−06	0.999
50 °C	0.0032	0.29	1.93e−05	0.996
60 °C	0.0028	0.17	1.05e−05	0.997
70 °C	0.0040	0.25	2.01e−05	0.994
80 °C	0.0019	0.12	5.94e−06	0.978
Sanchez		$p = 7$ bar		
55 °C	0.007	0.35	0.0001	0.991
65 °C	0.0017	0.08	3.889e−06	0.999
75 °C	0.0059	0.30	4.9e−05	0.995
De Groot		$p = 30$ bar		
50 °C	0.0075	0.45	0.00012	0.995
60 °C	0.0092	0.55	0.00013	0.994
70 °C	0.007	0.47	0.00011	0.995

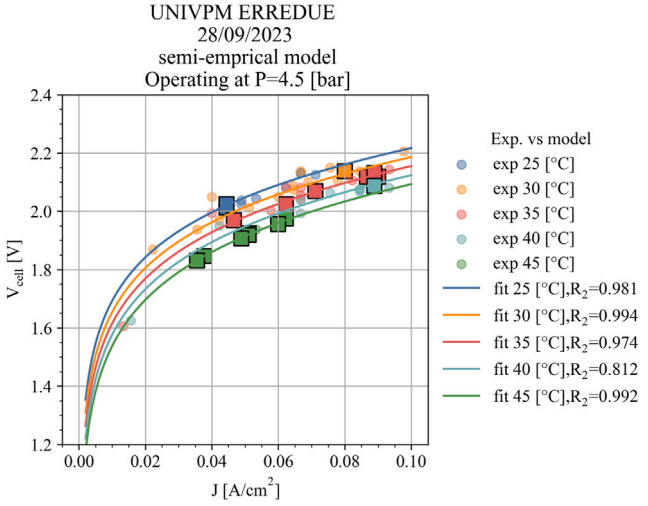

Fig. 10. Measured polarization curves from the NaOH-based electrolyte 23 kW electrolyzer together with model calibration.

The results of this investigation are shown in Fig. 12. The figure shows that indeed, when the temperature difference between the inlet and outlet of the electrolyzer stack exceeds 1 °C, the overall efficiency achieves the highest efficiencies of approximately 65% (LHV). Since the model keeps the voltage fixed as an input, these results indicate that temperature leveling inside the stack is indeed a preference as the energy consumption by the electrolyte pump, becomes nearly negligible when compared to the energy needed for the electrolysis. Furthermore, efficiency variations arise from comparing the two sources of power consumption. Higher voltages lead to greater thermal energy release, which in turn increases pump power consumption due to the need for a higher water flow rate to maintain the same temperature gap.

From an economic perspective, as depicted in Fig. 13, there exists a distinct zone where the levelized cost of hydrogen (LCOH) reaches a minimum value. This optimal range spans from 0.1 °C to 4 °C, regardless of the specific LCOE used. In contrast, LCOH is higher in the other zones. In the lower gap temperature zone, this is caused by the elevated operational cost attributed to the operational expenses of the water pump. Conversely, at the high gap temperature zone, lower inlet temperatures leads to a lower average current density, i.e. lower hydrogen production.

5. Conclusion

In this study, the impacts of the electrolyte flow rate in the thermal management of an alkaline electrolysis stack were investigated using a 1D model, which was compared with the 0D model formulation proposed by previous studies. The 1D model is based on a novel semi-empirical four-parameter alkaline water electrolysis cell mode

Table 6
Data from the semi-empirical model validation on the data from the ERREDUE 23 kW NaOH based electrolyzer.

Electrolyte	Experimental conditions			Calibrated parameters			
NaOH	p [bar]	T [° C]	wt [-]	δ_{el} [cm]	α [-]	$\frac{-E_a}{R}$ [K]	$ln(j_{0,ref})$ [ln($\frac{A}{cm^2}$)]
ERREDUE G6	4.5	25-30-35-40-45	0.18	0.56	0.06	−3501	5.06

Table 7
Calibrated model performance at different temperatures, for NaOH-based electrolyzer dataset.

	MAE [V]	MAPE [%]	RMSE [V]	R_2 [–]
ERREDUE G6	$p = 4.5$ bar			
25 °C	0.006	0.29	3.78e−05	0.981
30 °C	0.006	0.29	4.55e−05	0.994
35 °C	0.006	0.32	6.66e−05	0.974
40 °C	0.016	0.78	0.0003	0.812
45 °C	0.0033	0.17	1.6e−05	0.992

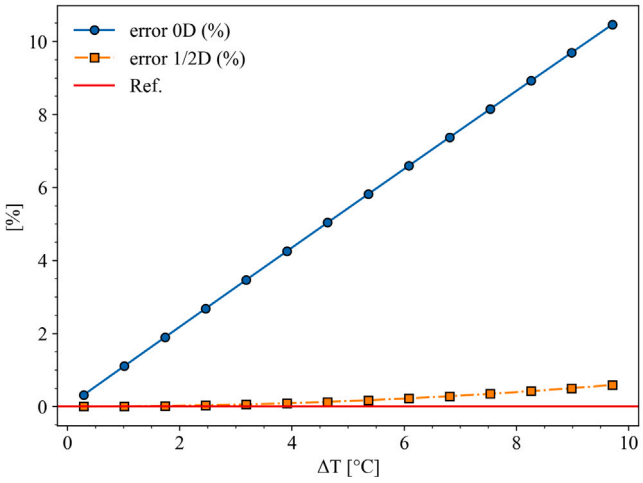

Fig. 11. Different scales of electrolyzer models' comparison, at different temperatures increase over the stack. Where error is the difference between the models' average current density, compared with the 1D model's average current density, in percentage.

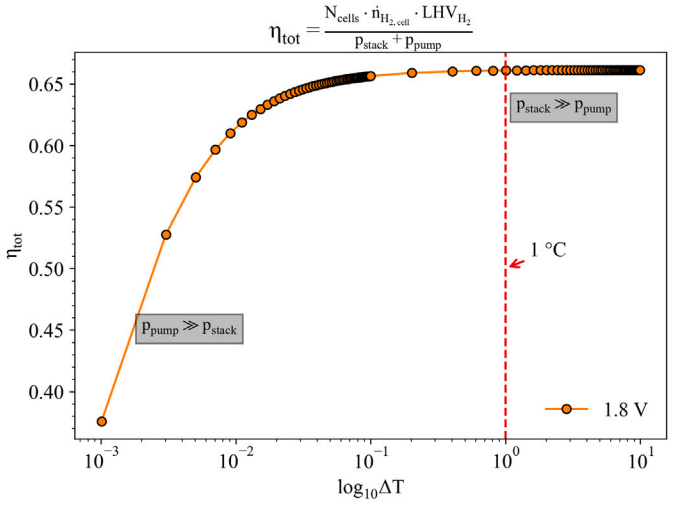

Fig. 12. Influence of temperature difference (inlet to outlet) in system efficiency, at different operating voltages. The outlet temperature is set as 80 °C.

that avoids limitations from previous studies, such as (i) fitting using non-absolute temperature (i.e., Celsius) (ii) polynomial temperature dependencies and (iii) material specific parameters (i.e., Nafion). Thus, the proposed model achieves simplicity (i.e., 4 fitting parameters) while still being accurate and general for multiple cell types.

In order to verify the improvements of the proposed model, its accuracy and robustness were validated through the use of four experimental datasets from the literature, covering a wide range of (i) operational parameters variation, (ii) cell area, and also (iii) electrolyte type. The results showed that all the data could be well represented ($R^2 \geq 0.9$) confirming the model ability to simulate the physical process at the most diverse conditions. Also with only six data points and considerable experimental noise, the model was shown to achieve a qualitatively reasonable representation ($R^2 \geq 0.81$). Moreover, despite of geometrical and operational differences, all datasets share a similar range for parameters (Table 4).

Moreover, the effects of model dimensionalities (i.e., 1D, 1/2D, and 0D) in the performance of alkaline electrolysis were investigated using numerical simulations. The results indicate that the 0D model showed significant errors in the performance, due to the temperature variation along the cell, while the 1/2D model achieved similar results to the 1D model (< 1% difference).

To investigate the performance at different flow rates, the cell-level model was assumed to be able to represent a stack, and this was embedded into a system-level model with a representation of heat exchangers and pumps. The temperature control was carried out by varying the electrolyte flow rate. This is at a cost of extra power for running the pumps and having larger auxiliary system components. Energy-wise there is thus a clear advantage of increasing the electrolyte flow rate, to have a low-temperature difference across the stack — close to the maximum allowable temperature, as this decreases the internal resistance of the cells. Very small temperature differences such as 1-4 °C are to be strived for. Economically, an optimal flow rate exists where losses from electrolyte pumping and lower hydrogen production due to higher gap temperature are harmonized. For the cases analyzed, although quantitative values oscillate, the qualitative trend of the LCOH does not change, despite different voltages and LCOEs. Specifically, LCOH can be 2–4 €/kg for the low LCOE case (30 €/MWh) and 4–6 €/kg for the high LCOE case (60 €/MWh).

In addition to the specific cases analyzed, several general insights can be drawn. Regardless of the LCOE or electrolyzer size, maintaining an outlet-to-inlet temperature difference of 1-4 °C is recommended for both technical and economic efficiency. And while the proposed

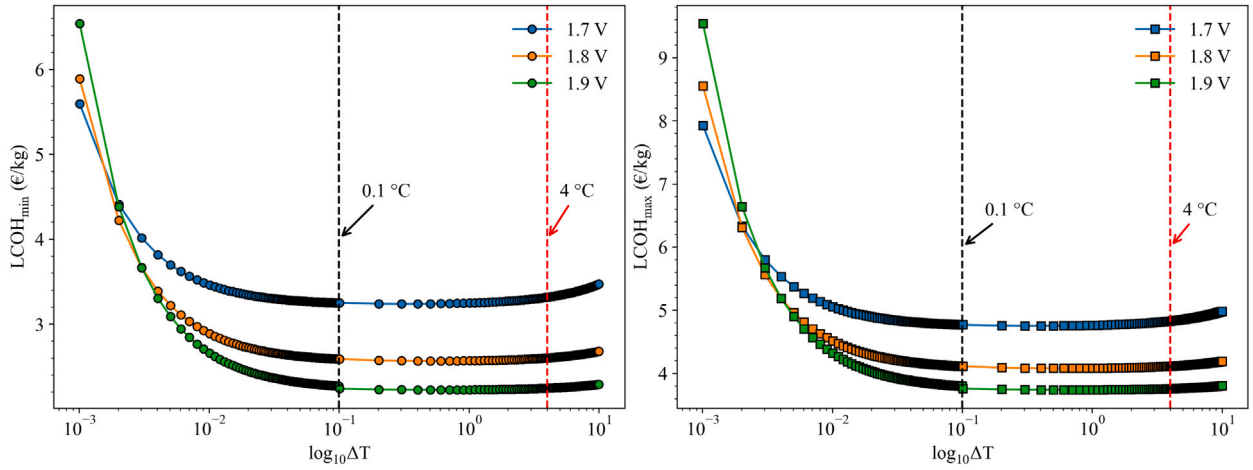

(a) LCOH with minimum LCOE (b) LCOH with maximum LCOE

Fig. 13. Influence of temperature difference (inlet to outlet) in the levelized cost of hydrogen. Outlet temperature set as 80 °C. Three distinct zones can be spotted: (i) high pump operational cost, (ii) optimal range and (iii) low hydrogen production zones.

system-level model holds significant potential, it is important to acknowledge its limitations. Indeed, once properly tuned, the model proved to be extremely fast to be solved, which makes it suitable to be adopted for holistic and systematic large-scale energy system analysis, as incorporating it in the optimization problem for both the planning (design phase) or scheduling stage (operational phase) of these systems. However, given that most energy system optimization commonly adopts Mixed Integer Linear Programming, the nonlinear nature of the model, necessary to include the required physical details of alkaline electrolysis, should be taken into account. Additionally, the formation of water vapor has been included in an implicit way, rather in a direct and comprehensive way. It is worth noting that these limitations are unlikely to alter the results discussed in this study. Nevertheless, the model proposed in this study can be improved by including the effects of bubbles, fluid mechanics, and gas diffusion across the membrane. Furthermore, the proposed model and its temperature control effects, however, are not validated for the NaOH electrolyzer, due to the technical bottlenecks, where at the current stage, it does not allow to change the water flow, nor does it have a pressure and temperature control yet, therefore, as future investigation, a refinement of the model, in addition to the validation of the temperature control, with the proper set-up adjustment, will be carried out.

Declaration of competing interest

The authors declare that they have no known competing financial interests or personal relationships that could have appeared to influence the work reported in this paper.

Data availability

Data will be made available on request.

References

[1] I. Staffell, D. Scamman, A. Velazquez Abad, P. Balcombe, P.E. Dodds, P. Ekins, N. Shah, K.R. Ward, The role of hydrogen and fuel cells in the global energy system, Energy Environ. Sci. 12 (2) (2019) 463–491, https://pubs.rsc.org/en/content/articlehtml/2019/ee/c8ee01157e.

[2] EU hydrogen strategy, 2022, URL https://energy.ec.europa.eu/topics/energy-systems-integration/hydrogen_en.

[3] S.A. Grigoriev, V.N. Fateev, D.G. Bessarabov, P. Millet, Current status, research trends, and challenges in water electrolysis science and technology, Int. J. Hydrog. Energy 45 (49) (2020) 26036–26058, http://dx.doi.org/10.1016/j.ijhydene.2020.03.109.

[4] W. Hug, H. Bussmann, A. Brinner, Intermittent operation and operation modeling of an alkaline electrolyzer, Int. J. Hydrog. Energy 18 (12) (1993) 973–977, URL https://www.sciencedirect.com/science/article/pii/036031999390078O.

[5] Ø. Ulleberg, Modeling of advanced alkaline electrolyzers: a system simulation approach, Int. J. Hydrog. Energy 28 (1) (2003) 21–33, http://dx.doi.org/10.1016/S0360-3199(02)00033-2.

[6] M. Hammoudi, C. Henao, K. Agbossou, Y. Dubé, M.L. Doumbia, New multi-physics approach for modelling and design of alkaline electrolyzers, Int. J. Hydrog. Energy 37 (19) (2012) 13895–13913, http://dx.doi.org/10.1016/j.ijhydene.2012.07.015.

[7] A. Ursúa, P. Sanchis, Static-dynamic modelling of the electrical behaviour of a commercial advanced alkaline water electrolyser, Int. J. Hydrog. Energy 37 (24) (2012) 18598–18614, http://dx.doi.org/10.1016/j.ijhydene.2012.09.125.

[8] J. Milewski, G. Guandalini, S. Campanari, Modeling an alkaline electrolysis cell through reduced-order and loss-estimate approaches, J. Power Sources 269 (2014) 203–211, http://dx.doi.org/10.1016/j.jpowsour.2014.06.138, URL https://www.sciencedirect.com/science/article/pii/S0378775314010027.

[9] K. Sandeep, S. Kamath, K. Mistry, A. Kumar M, S. Bhattacharya, K. Bhanja, S. Mohan, Experimental studies and modeling of advanced alkaline water electrolyser with porous nickel electrodes for hydrogen production, Int. J. Hydrog. Energy 42 (17) (2017) 12094–12103, URL https://www.sciencedirect.com/science/article/pii/S036031991731159X.

[10] M. Sánchez, E. Amores, L. Rodríguez, C. Clemente-Jul, Semi-empirical model and experimental validation for the performance evaluation of a 15 kW alkaline water electrolyzer, Int. J. Hydrog. Energy 43 (45) (2018) 20332–20345, http://dx.doi.org/10.1016/j.ijhydene.2018.09.029.

[11] J. Haverkort, H. Rajaei, Voltage losses in zero-gap alkaline water electrolysis, J. Power Sources 497 (2021) 229864, URL https://www.sciencedirect.com/science/article/pii/S037877532100402X.

[12] D. Jang, W. Choi, H.S. Cho, W.C. Cho, C.H. Kim, S. Kang, Numerical modeling and analysis of the temperature effect on the performance of an alkaline water electrolysis system, J. Power Sources 506 (2021) http://dx.doi.org/10.1016/j.jpowsour.2021.230106.

[13] M.T. de Groot, J. Kraakman, R.L. Garcia Barros, Optimal operating parameters for advanced alkaline water electrolysis, Int. J. Hydrog. Energy 47 (82) (2022) 34773–34783, http://dx.doi.org/10.1016/J.IJHYDENE.2022.08.075.

[14] R.L. Leroy, C.T. Bowen, D.J. LeRoy, The thermodynamics of aqueous water electrolysis, J. Electrochem. Soc. 127 (1980) 1954–1962, URL https://api.semanticscholar.org/CorpusID:97628747.

[15] J. Balej, Water vapour partial pressures and water activities in potassium and sodium hydroxide solutions over wide concentration and temperature ranges, Int. J. Hydrog. Energy 10 (4) (1985) 233–243, http://dx.doi.org/10.1016/0360-3199(85)90093-X, URL https://www.sciencedirect.com/science/article/pii/036031998590093X.

[16] R.L. LeRoy, C.T. Bowen, D.J. LeRoy, The thermodynamics of aqueous water electrolysis, J. Electrochem. Soc. 127 (9) (1980) 1954, http://dx.doi.org/10.1149/1.2130044.

[17] R.J. Gilliam, J.W. Graydon, D.W. Kirk, S.J. Thorpe, A review of specific conductivities of potassium hydroxide solutions for various concentrations and temperatures, Int. J. Hydrog. Energy 32 (3) (2007) 359–364, http://dx.doi.org/10.1016/j.ijhydene.2006.10.062.

[18] D. Le Bideau, P. Mandin, M. Benbouzid, M. Kim, M. Sellier, Review of necessary thermophysical properties and their sensivities with temperature and electrolyte mass fractions for alkaline water electrolysis multiphysics modelling, Int. J. Hydrog. Energy 44 (10) (2019) 4553–4569, http://dx.doi.org/10.1016/j.ijhydene.2018.12.222, URL https://www.sciencedirect.com/science/article/pii/S0360319919300175.

[19] P. Vermeiren, W. Adriansens, J.P. Moreels, R. Leysen, Evaluation of the zirfon® separator for use in alkaline water electrolysis and Ni-H2 batteries, Int. J. Hydrog. Energy 23 (5) (1998) 321–324, http://dx.doi.org/10.1016/s0360-3199(97)00069-4.

[20] C. Henao, K. Agbossou, M. Hammoudi, Y. Dubé, A. Cardenas, Simulation tool based on a physics model and an electrical analogy for an alkaline electrolyser, J. Power Sources 250 (2014) 58–67, http://dx.doi.org/10.1016/j.jpowsour.2013.10.086.

[21] H. Vogt, R.J. Balzer, The bubble coverage of gas-evolving electrodes in stagnant electrolytes, Electrochim. Acta 50 (10) (2005) 2073–2079, http://dx.doi.org/10.1016/j.electacta.2004.09.025.

[22] B.J. McBride, M.J. Zehe, S. Gordon, NASA Glenn Coefficients for Calculating Thermodynamic Properties of Individual Species: National Aeronautics and Space Administration, (September) John H. Glenn Research Center at Lewis Field, 2002, p. 295, https://ntrs.nasa.gov/citations/20020085330.

[23] I.D. Zaytsev, G.G. Aseev, Properties of Aqueous Solutions of Electrolytes, vol. 30, (08) American Library Association, 1992, pp. 30–4415.

[24] G. Van Rossum, F.L. Drake, Jr., Python Reference Manual, Centrum voor Wiskunde en Informatica Amsterdam, 1995.

[25] T. pandas development team, pandas-dev/pandas: Pandas, Zenodo, 2020, http://dx.doi.org/10.5281/zenodo.3509134.

[26] P. Virtanen, R. Gommers, T.E. Oliphant, M. Haberland, T. Reddy, D. Cournapeau, E. Burovski, P. Peterson, W. Weckesser, J. Bright, S.J. van der Walt, M. Brett, J. Wilson, K.J. Millman, N. Mayorov, A.R.J. Nelson, E. Jones, R. Kern, E. Larson, C.J. Carey, İ. Polat, Y. Feng, E.W. Moore, J. VanderPlas, D. Laxalde, J. Perktold, R. Cimrman, I. Henriksen, E.A. Quintero, C.R. Harris, A.M. Archibald, A.H. Ribeiro, F. Pedregosa, P. van Mulbregt, SciPy 1.0 Contributors, Scipy 1.0: Fundamental algorithms for scientific computing in python, Nature Methods 17 (2020) 261–272, http://dx.doi.org/10.1038/s41592-019-0686-2.

[27] F. Pedregosa, G. Varoquaux, A. Gramfort, V. Michel, B. Thirion, O. Grisel, M. Blondel, P. Prettenhofer, R. Weiss, V. Dubourg, J. Vanderplas, A. Passos, D. Cournapeau, M. Brucher, M. Perrot, E. Duchesnay, Scikit-learn: Machine learning in python, J. Mach. Learn. Res. 12 (2011) 2825–2830.

[28] G. Sakas, A. Ibáñez-Rioja, V. Ruuskanen, A. Kosonen, J. Ahola, O. Bergmann, Dynamic energy and mass balance model for an industrial alkaline water electrolyzer plant process, Int. J. Hydrog. Energy 47 (7) (2022) 4328–4345, http://dx.doi.org/10.1016/J.IJHYDENE.2021.11.126.

[29] S. Krishnan, V. Koning, M. Theodorus de Groot, A. de Groot, P.G. Mendoza, M. Junginger, G.J. Kramer, Present and future cost of alkaline and PEM electrolyser stacks, Int. J. Hydrog. Energy 48 (83) (2023) 32313–32330, http://dx.doi.org/10.1016/j.ijhydene.2023.05.031, URL https://www.sciencedirect.com/science/article/pii/S0360319923022590.

[30] H. Nami, O.B. Rizvandi, C. Chatzichristodoulou, P.V. Hendriksen, H.L. Frandsen, Techno-economic analysis of current and emerging electrolysis technologies for green hydrogen production, Energy Convers. Manage. 269 (2022) http://dx.doi.org/10.1016/j.enconman.2022.116162, URL https://linkinghub.elsevier.com/retrieve/pii/S0196890422009438.

[31] R. Peters, W. Tiedemann, I. Hoven, R. Deja, N. Kruse, Q. Fang, D. Schäfer, F. Kunz, L. Blum, R. Peters, R.-A. Eichel, Experimental results of a 10/40 kW-class reversible solid oxide cell demonstration system at Forschungszentrum Jülich, J. Electrochem. Soc. 170 (4) (2023) 044509, http://dx.doi.org/10.1149/1945-7111/accbf0, URL https://iopscience.iop.org/article/10.1149/1945-7111/accbf0.

[32] C.A. Hunter, M.M. Penev, E.P. Reznicek, J. Eichman, N. Rustagi, S.F. Baldwin, Techno-economic analysis of long-duration energy storage and flexible power generation technologies to support high-variable renewable energy grids, Joule 5 (8) (2021) 2077–2101, http://dx.doi.org/10.1016/j.joule.2021.06.018, URL https://linkinghub.elsevier.com/retrieve/pii/S2542435121003068.

[33] European Central Bank, Euro foreign exchange reference rates, 2023, URL https://www.ecb.europa.eu/stats/policy_and_exchange_rates/euro_reference_exchange_rates/html/index.en.html.

[34] R. Turton, R.C. Bailie, W.B. Whiting, J.A. Shaeiwitz, Analysis, Synthesis, and Design of Chemical Processes, 3th ed, Prentice Hall, Upper Saddle River, NJ, 2009.

[35] Eurostat, Labour cost levels by NACE Rev. 2 activity, 2024, http://dx.doi.org/10.2908/LC_LCI_LEV.

[36] R.H. Perry, D.W. Green, J.O. Maloney (Eds.), Perry's Chemical Engineers' Handbook, Seventh ed., McGraw-Hill, New York, 1997.

[37] European Central Bank, Inflation and consumer prices, 2023, URL https://www.ecb.europa.eu/stats/macroeconomic_and_sectoral/hicp/html/index.en.html.

[38] ABB, Advant controller AC500: Intelligent decentralized automation system, URL https://new.abb.com/plc/it/controllori-logici-programmabili-plc/ac500.

[39] E. GAS, G6 – generatore di idrogeno e ossigeno con sistema di depurazione e miscelatore di gas per trattamenti termici, 2024, URL https://www.erreduegas.it/installazioni/g6-generatore-di-idrogeno-e-ossigeno-con-sistema-di-depurazione-e-miscelatore-di-gas-per-trattamenti-termici/. (Accessed 27 February 2024).

[40] F. Mennilli, L. Jin, M. Rossi, G. Comodi, Assessment of a NaOH-based alkaline electrolyser's performance: System modelling and operating parameters optimisation, Int. J. Hydrog. Energy 85 (2024) 625–634, http://dx.doi.org/10.1016/j.ijhydene.2024.08.175, URL https://www.sciencedirect.com/science/article/pii/S0360319924033342.